Egyptian Geophysical Society
EGS Journal, Vol. 8, No. 1, 1-11 (2010)

APPLICATION OF UPWARD CONTINUATION AND EULER DECONVOLUTION ON AEROMAGNETIC DATA TO DELINEATE THE REGIONAL STRUCTURAL FRAMEWORK OF GABAL EL MOGARID AREA, SOUTH EASTERN DESERT, EGYPT.

R.M. Abdelrahiem
Nuclear Materials Authority, P.O. Box 530, El-Maadi, Cairo, Egypt.

تطبيق طريقتى الاستمرارية لاعلى ومحور اويلر على بيانات المسح المغناطيسى الجوى لتقدير الوضع التركيبى لجبل المجرد- جنوب الصحراء الشرقية-مصر

الخلاصة: يقع جبل المجرد فى جنوب الصحراء الشرقية مصر ويغطى حوالى ٨٤٠ كم٢. تغطى المنطقة بصخور الكمبرى النارية والمتحولة ويتراكب فوقها الحجر الرملى النوبى الكريتاوى ورواسب الوديان من العصر الثلاثى والرباعى وتظهر المنطقة بعض الشاذات الأشعاعية المرتبطة بصخور الجرانيت ويحكمها نظام فوالق تتجه فى اتجاهات الشمال شمال غرب، الشمال الغربى، الشمال الشرقى. لقد عولجت البيانات المغناطيسية وتم فصل مركبتين للشاذات المغناطيسية احدهما قريبة من السطح على عمق ٠,٨ كم والثانية عميقة اقليمية على عمق ١,٦ كم . ولتتبع الخواص المغناطيسية للشاذات تم فصل البيانات المغناطيسية ومتابعتها إلى اعلى عند ١ ، ١,٥ ، ٢ ، ٢,٥ كم ومن تحاليل البيانات المغناطيسية لمعرفة التراكيب الموجودة و الحدود و العروق اظهرت الخرائط اعماق محددة ومن خلال تكامل المعلومات المغناطيسية أمكن رسم الوضع التركيبى للمنطقة ولقد اوضحت الخرائط التركيبية المفسرة من البيانات المغناطيسية ان الخطوط التركيبية تزداد على السطح وتقل اكثر فى العمق وقد اظهرت الفوالق الكتل الهابطة والكتل الصاعدة حولها وقد كانت الفوالق الأقليمية العميقة تتجه غالبا فى اتجاهات شمال–جنوب–شرق غرب وشمال شرق بينما الفوالق الضحلة والسطحية تتميز بشكل الموزيك وتاخذ اتجاهات عدة منها شمال شمال غرب، شمال–جنوب وشمال شرق.

ABSTRACT: *Gabal El Mogarid area is located in the south Eastern Desert of Egypt, between latitudes 23° 30' & 23° 45' N and longitudes 33° 12' & 33° 30'. It covers a total surface area of about 840 Km^2. The area is mainly covered by Precambrian igneous and metamorphic rocks overlain by Cretaceous Nubian Sandstone, Tertiary sediments and Quaternary wadi deposits. This area shows some radioactive anomalies related to the granitic rocks and is structurally controlled by the dominated fault system, which trending in the NNW, NW and NE directions.*

Two main average magnetic interfaces at depths 0.8 and 1.6 km below the measuring level were calculated through the application of the two-dimensional local power spectrum technique of the RTP magnetic map. Filtering of the aeromagnetic data at the two interfaces was conducted to assist the discrimination between the shallow source (near-surface or residual) and deep source (deep-seated or regional) magnetic anomalies.

Upward continuation was carried out at four different levels (1.0, 1.5, 2.0 and 2.5 km) to follow the variations of the magnetic characters of anomalies, when passing from shallow to deep levels. On the other hand, the structural delineations that come from the application of extended Euler deconvolution technique as magnetic contacts or sills and dykes revealed in the area at specified depths. The information obtained from the interpretative techniques (regional, residual, upward continuation and Euler deconvolution) were applied and integrated to construct a basement tectonic map.

The interperated structural maps show a gradual increase in the density and crowdness of the interpreted magnetic structural lineaments upwardly from the deep-seated interface the near-surface interfaces. The structural elements affecting to basement complex at the two assigned interfaces with faults (subsided and uplifted blocks) are delineated. This study revealed the existence of several sets of faults the regional (deep-seated) faults are expressed mainly by N-S, E-W and NE trending faults. Meanwhile, the residual (near-surface) lineaments are characterized by a mosaic pattern and shows different sets of faults mainly trending in the NNW, N-S, NW and NE directions.

1- INTRODUCTION

The present work is dedicated to delineate the subsurface structural framework affected the study area, to follow up the radiospectrometric anomalies. This was achieved through the integration of some geophysical interpretation techniques applied to the aeromagnetic survey data. Gabal El Mogarid area is located in the south Eastern Desert of Egypt, between latitudes 23° 30' & 23° 45' N and longitudes 33° 12' & 33° 30' E. It covers a total surface area of about 840 Km^2 (Fig. 1).

The area under consideration is characterized by low relief topography. The general outlines of the topography of the investigated area shows that, it is mainly covered by Cretaceous sediments forming low hills, while the basement complex rocks form relatively high and rugged mountains. The highest and prominent peaks characterizing the area under study (Fig.2) are those of Gabal (Mountain) Agib (563 m) and Gabal El Mogarid (374 m). Also, the area is dissected by a large group of wadis (valleys), as Wadi Arab and Wadi Um

Herbal. The main wadis trend in approximately three main directions, NW-SE, NE-SW and WNW-ESE.

2- Geologic outlines and structural setting:

The basement complex, covering Gabal El Mogarid area is almost composed of igneous, metamorphic and sedimentary rocks ranging in age from Precambrian to Quaternary. The succession of the different rock types is related to the basement rocks and Tertiary sediments, as well as the Cretaceous Nubian Sandstone. Quaternary (recent) deposits are represented by wadi deposits, which cut through the other rocks and are composed of detritus sands, gravels, pebbles and rare boulders, that are generally formed by weathering of the previously existing basement rocks.

The distributions of the different exposed different rock types are shown on the compiled geologic map (Fig.3). This map was compiled from various sources, mainly through the photogeologic map prepared by Hunting, 1967 and the geologic map of Aswan area prepared by Conoco, 1987. The rocks have been subjected – since their formation – to different tectonic cycles during the long period of the geologic history. Accordingly, the effect of these tectonic movements resulted in the complexity of the structure of the study area.

Gabal Agib Ring Complex is located in the northwestern part of the study area, to the west of Gabal Agib (Fig.4). The relief of the ring complex is high, where the contour lines in the topographic map show that, the area occupied by the ring complex has a general elevation of 350 m, above sea level and the highest point in the ring reaches 440 m. The country rocks surrounding the complex are mainly represented by the coarse grained granites and quartz syenites in the form of large dykes crossing the coarse granites. The coarse grained granite become more syenitic at the northern part of the ring.

The ring is cut by a number of radial faults along the main tributaries with two main trends namely the NW-SE and NE-SW trends. Linear faults strike E-W and are considered as a younger set crossing all the dykes striking NE-SW and NW-SE.

The rhyolites and diabase rocks are affected by some of the radial faults, and the syenites masked these faults. The E-W faults affected the syenitic rocks (Mansour, 1985). The tectonic framework of the ring complexes in the Eastern Desert is governed by the configuration of both the basement blocks and the rift structures. Ring complexes tend to occur in the form of chains extending parallel to the main structural trends. Thus, both the Eriythrean and the Abyssinian trends and particularly their points of intersections play an important role in the distribution of the ring complexes in Egypt.

The succession in the ring complex is as follows, from older to younger (after Mansour, 1985):

- Country rocks composed mainly of coarse grained granites.
- Tectonic activity resulting of radial faults and ring dykes of rhyolites, trachytes and diabase.
- An intrusion of syenitic magma at the top of all the previously mentioned rocks.

The contact between the outer ring and the central mass is normal and of intrusive nature. On aerial photographs, this contact is distinct and clear, due to the differences in tone and surface texture between the country rocks and the rock of the ring complex. The rocks in the outer ring are darker in tone and coarser in surface texture than those in the central part of the ring.

The tectonic pattern of the area is the result of the combined effect of successive earth movements, that took place since the Precambrian time until now. There are three main regional fault trends in the area, the sequence of which is NE-SW, E-W, NW-SE and N-S (El Shazly, 1966).

3- The airborne geophysical survey:

The airborne geophysical survey of the study area was carried out by Aero Service Division, Western Geophysical Company of America in 1984. It involved an aeroradiometric survey over the majority of the Eastern Desert of Egypt, between the River Nile and the Red Sea Coast. The aeromagnetic and aerospectrometric surveys were conducted along nearly parallel flight lines, that were oriented in the NE-SW direction at one kilometer spacing intervals perpendicular to the main geology, and structure of the surveyed area. Meanwhile, the tie lines were flown in the NW-SE direction at 10 Km intervals at a nominal flight altitude of 120 m ground clearance, using twin-engine Cessna-404, Titan type aircraft. The aerial magnetic and gamma-ray spectrometric measurements were made using a continuously recording airborne varian V-85 proton precession magnetometer (sensitivity of 0.1 nanotesla "nt") mounted in a tail stinger configuration and a high sensitivity 256 channel airborne gamma-ray spectrometer, with a primary 50.3 liters Sodium Iodide and Thaiium activated (NaI "TI") detector array. The obtained airborne gamma-ray spectrometric and magnetic data were reduced, compiled and finally presented in the form of contoured map at scale of 1 : 50,000.

IV- The relation between magnetic and radioactive methods :

The Uranium, Thorium and Potassium are the hydrothermal solution and always found in the structural features (as faults and fractures), and the magnetic method showing these structural features may extend in the depth or not. In the study area, most of the identified radioactive anomalies in Gabal El Mogarid are confined to high topographic and related to NNW, NW and NE fault trends, which affecting the distribution of the radioactive elements (Figs.5 and 6).

This may attract the attention to potential and structurally controlled Uranium and/or Thorium mineralization. Such faults can act as channel ways for mineralizing solutions.

Some agreement of the structural lineaments, especially the NNW, NW and NE fault trends from the total count map (Fig.5) and the RTP magnetic map (Fig.8). These faults may be extend at depth. Meanwhile, some other fault trends do not agree with the magnetic lineaments, which may represent the surface structural lineaments.

5- Geophysical Data Processing Techniques and Interpretation:

The structural framework of the study area was delineated through the application and integration of some interpretative techniques on the aeromagnetic data reduced to the north magnetic pole (RTP) map.

(1) Reduction to the North Magnetic Pole (RTP):

To reduce the influence of inclination of the earth's magnetic field on the shapes, sizes and locations of anomalies, reduction to the north magnetic pole of the aeromagnetic data has been carried out, as referred earlier. This reduction helped to assess more accurately the magnetized sources, and to identify the significant magnetic zones of anomalies of unusual amplitudes and gradients.

A general outlook on the RTP aeromagnetic intensity map (Fig.8), in comparison with the original total field intensity aeromagnetic map (Fig.7) reflects the northward shift in the positions of the inherited magnetic anomalies, due to the elimination of the inclination of the magnetic field at the study area. Besides, the number of anomalies becomes somewhat larger with comparable decrease of their areal extension and increase of their magnetic relief's. The magnetic gradients of the RTP magnetic anomalies become more intense and steep, giving rise to more accurate resolution and delineation of both the encountered lithologic and structural features.

Careful examination of the RTP magnetic map (Fig.8) showed that, the investigated area is characterized by the presence of groups of numerous positive and negative magnetic anomalies of varying wavelengths, amplitudes, shapes, sizes and magnitudes, according to the types and depths of source bodies.

Three magnetic anomalous zones were distinguished on the bases of the differences in the magnitudes and characters of magnetic anomalies (wavelengths, amplitudes, areal distributions and trend patterns of the anomalies). The first anomalous zone is occupied by a broad belt of positive magnetic anomalies and takes the NNW to NW and E-W trends.

This zone is located in the northern and southwestern parts of the study area and is associated with metasediments, Cretaceous sediments and granitic rocks. It has low to moderate frequencies and relatively moderate amplitudes. The magnetic amplitudes decrease gradually towards the central part of the study area, which may suggest their association with deep-seated basic source.

The second magnetic zone covers the northern and southeastern parts of the study area. This zone is represented by many moderate to strong negative magnetic anomalies aligned mainly in the NNW and N-S trends. It is associated mainly with Cretaceous sediments. The high amplitudes and frequencies of these anomalous zone, may suggest their association with shallow acidic sources.

The third magnetic zone shows a limited distribution. It occupies the south-central part (mid) of the study area and is composed mainly of negative magnetic anomaly. On the surface, this magnetic zone is connected with Quaternary deposits and takes the NW-SE trend.

(2) Calculation of spectral frequency analysis:

Filtering techniques, that include high and low-pass filters, were applied in order to recognize the shallow and deep sources responsible for the residual and regional fields. Isolating the regional and residual magnetic anomalies in the studied area was carried out using the band-pass filter technique.

Potential field data (e.g., aeromagnetic data), can be represented by two-dimensional Fourier series consisting of various frequencies, which can characterize the present anomalies (Curits and Jain, 1975). In the present study, the Fast Fourier Transform (FFT) was applied on the RTP aeromagnetic survey data to calculate the energy spectrum. As a result, a two-dimensional power spectrum curve was obtained (Fig.9). Based on the appearance of the spectrum, i.e. changes in the slope of the spectrum curve, the spectrum is divided into two components, the deep origin or the regional (deep-seated) component dominates the low frequency or the long wavelength part of the spectrum, and the shallow origin or the near-surface component dominates the high frequency or the short wavelength part of the spectrum. Two main average levels (interfaces) at depths 0.8 and 1.6 km below the measuring level were calculated and revealed on the spectrum curve for the near-surface and deep-seated magnetic components, respectively.

(3) Separation of magnetic anomalies:

Depending upon the results of analysis of the energy spectrum of the aeromagnetic data of the study area, the band-pass filter technique for separation was applied to the RTP aeromagnetic data to produce the regional and residual magnetic-component maps at the two assigned interfaces (Figs. 10 & 11), respectively. The residual map focuses the attention on weaker features, which are obscured by the stronger regional effects on the original map (Telford et al., 1990).

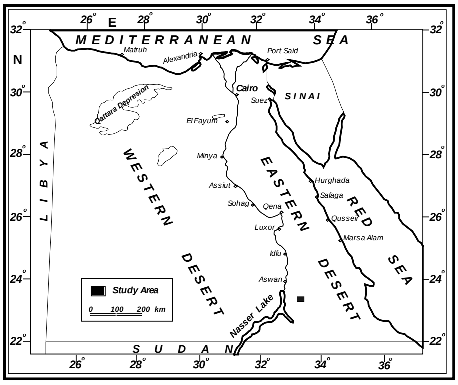

Fig. (1): Location map of Gabal El-Mogarid Area, South Eastern Desert, Egypt.

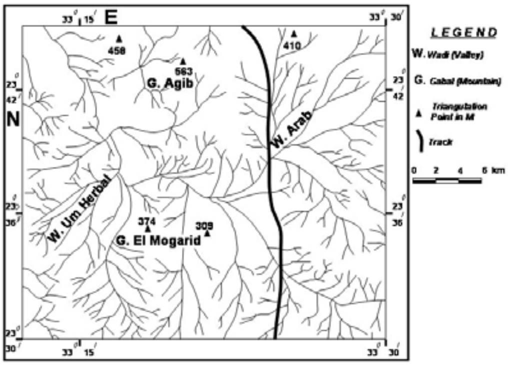

Fig. (2): Topographic map of Gabal El-Mogarid Area, South Eastern Desert, Egypt.

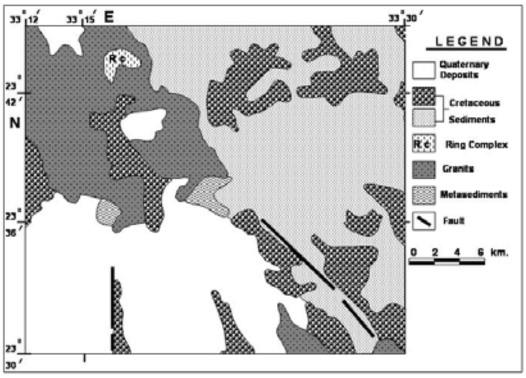

Fig. (3) Compiled Geological Map of G. ELmogarid Area, South Eastern Desert, Egypt.Mansour, 1985)

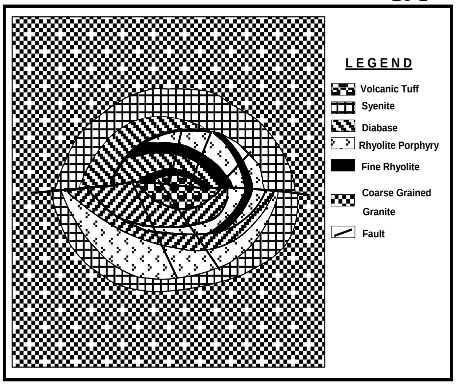

Fig . (4) Field Sketch of G.Agib Ring complex , South Eastern Desert Egypt (after Mansour,1985)

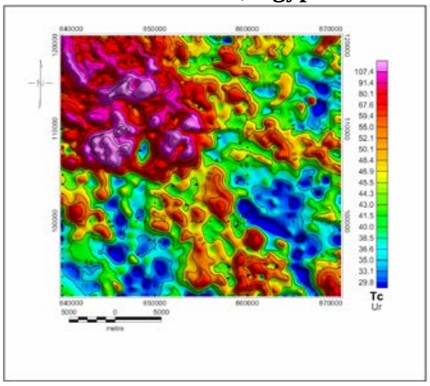

Fig. (5): Fill colored contour map of Total Count (T.C. in Ur.), G. ELmogarid Area , South Eastern Desert, Egypt.

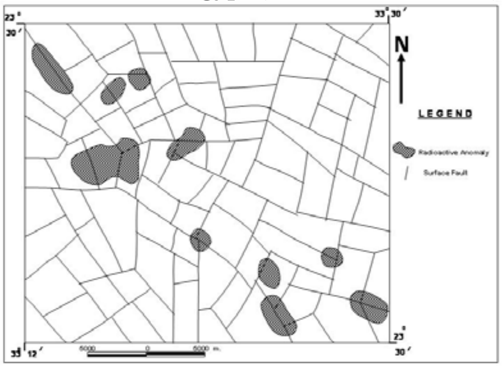

Fig. (6): Identified Radioactive Anomalies in relation to the surface Faulting pattern, G. ELmogarid Area, South Eastern Desert, Egypt.

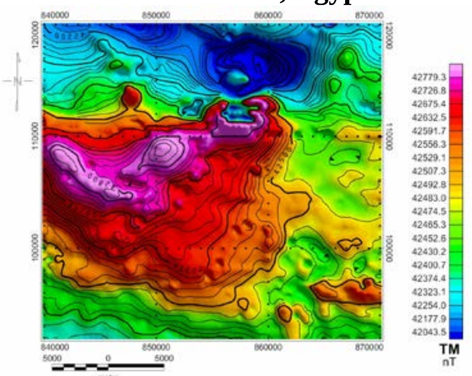

Fig. (7): Total intensity aeromagnetic contour map, G. ELmogarid Area,South Eastern Desert, Egypt.

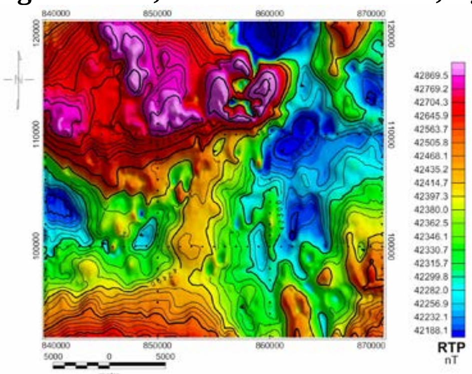

Fig. (8): Reduced to pole (RTP) aeromagnetic contour map, G. ELmogarid Area, South Eastern Desert, Egypt.

The residual magnetic-component map (Fig. 11) clearly shows several clusters of positive and negative magnetic anomalies, which are of higher resolution than that of the RTP aeromagnetic map. These anomalies have nearly semicircular and elongated shapes and are characterized by their relatively high frequencies and short wavelengths. The local variations in both frequency and amplitude of these anomalies may be due to the differences in their composition and/or their relative depths of their sources. These major trends, NNW-SSE, E-W, N-S, NW-SE and NE-SW directions, are distinguished for the near-surface structures in the study area, as deduced from the residual map.

On the contrary of the high frequency and short wavelength magnetic anomalies, which are observed on the residual magnetic-component map, the regional magnetic anomalies are of low frequencies and long wavelengths. The near-surface magnetic component map (Fig.11) shows several alternating positive and negative magnetic anomalies, which possessing a general NNW, N-S, E-W and NE directions. The local variations in both frequency and amplitude of these anomalies may be due to the difference in their composition and/or their relative depths to their sources. The regional deep-seated magnetic component map (Fig.10) shows deep-seated high amplitude positive and negative magnetic anomalies.

Careful examination of the regional magnetic-component map (Fig. 10) indicates that, some of the magnetic anomalies continue to appear from the RTP magnetic map (Fig. 8) to the regional magnetic-component map (Fig. 10), but with lower amplitudes and frequencies at the deep-seated interface. These anomalies could be interpreted as of deep-seated origin. Moreover, a group of small-sized magnetic anomalies, shown on the RTP map (Fig.8), appears also on the regional magnetic-component map, but as single continuous and broad magnetic anomalies. These features indicate that, these small-sized anomalies have a common deep root and, therefore, could be considered of deep-seated origin. Some other magnetic anomalies disappeared on the regional magnetic-component map. Meanwhile, they are manifested on both the RTP aeromagnetic and the residual magnetic-component maps (Fig. 11). These phenomena can serve as a criterion that, these anomalies originate from near-surface magnetic sources located at shallow depths. The regional magnetic-component map brings out the major trends affecting the deep-seated structures of the study area. These structures nearly possess the NNW-SSE, NE-SW and E-W, as the main structural trends, beside the NW-SE and N-S trends, but in less significant order.

(4) Upward Continuation:

Upward continuation tends to accentuate anomalies caused by deep sources at the expense of anomalies caused by shallow sources (Blakely, 1995). It may be desirable to remove or smooth out the localized disturbances caused by features of small lateral extent, so as to bring out large-scale structures more clearly and giving a clearer picture of the regional field (Tasy, 1975). In the present study, the upward continuation process of the magnetic anomalies was carried out for the reduced to pole aeromagnetic map (Fig.8),using the coefficients computed by numerical evaluation of the Fourier transform in the frequency domain. The computation was conducted on four different levels applying varying grid cell units (grid spacing), which are compatible with 1.0, 1.5, 2.0 and 2.5 km average depths. Geosoft software geophysical package (1994) is used for this computation. Consequently, four maps (Figs.12 to 15) were drawn at the afore-mentioned levels, respectively.

Comparative investigation of the RTP continued upward aeromagnetic map at level 1.5 km (Fig.12) and the regional magnetic-component map at interface 1.8 km (Fig.10) shows that, there is a great similarity between both of them. However, at this level of observation, the magnetic anomalies on the two maps still have approximately the same characteristics, both in anomaly wavelength, and areal distribution, as well as magnetic, in trend which most of the residual bodies are removed. The difference in magnitudes of the magnetic anomalies in some parts may be due to the difference in algorithm of the software used for the calculation of the two processes. Consequently, the contours of the two maps nearly agree well with the ideal response as to shape, however, the amplitude of the contours is relatively displaced by one or multiple of the basic contour interval.

The upward continued map at level 1.5 km (Fig. 13) shows the existence of high and low magnetic zones, nearly at the same localities that have been observed on the upward continued map at level 1.0 km (Fig.12). Some of these magnetic anomalies are shown to be limited in extension at depth 1.5 km (Fig.13). Moreover, some other anomalies disappear on the upward continued map at the third and fourth levels (2.0 & 2.5 km) of Figs. (14 & 15). Meanwhile, they are still found on both the first and second upward continued maps (Figs. 12 & 13). According to this observation, these magnetic anomalies could be originated from depths of more than 1.5 km and less than 2.5 km and are, therefore, considered near-surface anomalies possessing shallow roots. The close inspection of the four upward continued maps (Figs.12 to 15) shows that, some of the low (or high) magnetic zones decrease in their areal extent on the account of the high (or low) magnetic zones by increasing the depth of observation. This may offer strong evidence to the compositional differences of the underlying rocks by increasing depth.

The upward continued aeromagnetic map at level 2.5 km (Fig.15) shows the broad effects of the proper deep-seated magnetic features including the structural and lithological variations within the basement (intrabasement) allover the area under investigation, that continue to appear from the original RTP aeromagnetic map. So, the sources of magnetic anomalies appearing on this map may indicate that, they are deeply-rooted and either reach the ground surface or at a relatively shallow depth.

The upward continued aeromagnetic maps at levels 2.0 and 2.5 km (Figs.14 & 15) show that, the study area can be divided into two magnetic zones. The first magnetic zone has high magnetic characters and found in the western part (uplifted block) and the second has low magnetic characters and occupies the eastern part of the study area (subsided block). This subsided block is dissected by two normal faults, which trending in the NE-SW direction and separated from the uplifted block by NW-SE fault trend. The uplifted block in the western part is dissected by two E-W normal faults. These faults divided these uplifted blocks into three smaller blocks; two of them are uplifted blocks in the northern and south eastern parts.

Meanwhile, the third is a subsided block lies between the two uplifted blocks and reflecting a graben shape (Figs.14 & 15).

The general view of these deep-seated magnetic anomalies, when passing from the first to the fourth level maps, shows that, their areal extent becomes wider and broader in the subsurface due to their long wavelengths and hence low frequencies, which-thus-results in smoother magnetic contours and less resolution (Kearey and Michael, 1994). Besides, their magnitudes were minimized and reached their minimal values at the third specified level (2.5 km depth) which represents the deepest one.

The northwestern part of the study area shows a large extension in depth of more than 2.0 and 2.5 km. The two upward continued maps at 2.0 and 2.5 km (Figs.14 & 15) exhibit also that, these large masses are bounded and separated from the others by major faults.

The predominant structural trends deduced from the four upward continued magnetic maps (Figs.12 to 15) are the NW-SE, NE-SW and E-W directions. Therefore, they are expressed as deep-seated features in the study area.

(5) Euler Deconvolution:

The use of Euler deconvolution, as an interpretation method applied to potential field data, is well established to give the source position and its depth rapidly by deconvolution (Reid, 1995). The method uses potential field data, which are in grid form. The Euler's homogeneity equation relates the magnetic field and its gradient components to the location of the source with the degree of homogeneity N, which may be interpreted as a particular structural index. The structural index is a measure of the rate of change of a field with distance, for example, a magnetic field for a contact has a structural index N=0, while for a fault N=0.5, for a dyke/sill N=1. etc. However, in most practical cases even though, the structural index is for a particular geometry, the solution may outline sources with other structural indices. The Euler's equation is given by:

$$(x-x_0) \,.\, \delta T/\delta x + (y-y_0) \,.\, \delta T/\delta y + (z-z_0) \,.\, \delta T/\delta z = N(B-T)$$

where: (x_0 ,y_0 & z_0) is the position of the source, with structural index N, whose total field T is measured at (x, y & z) and the total field has its regional value B.

The optimum source location is found by the least square inversion of the data within a chosen window length. Solutions are generally obtained for different structural index values and the solutions with best clustering of the data are selected. With smaller grid intervals, the solutions were found to be noisy. The Euler solution presented here is for grid interval of 0.5 km.

In the present study, the extended Euler deconvolution was run twice; one with a structural index (N) of (0) to identify the magnetic contacts, and the other with (N) equal (1.0) to identify the sills and dykes. The deduced results for the magnetic contacts are shown in Fig. (16) and those for the sills and dykes in Fig.(17), in addition to the conventional clustering of solutions of depths along the entire area. The two maps show roughly the same trends for the two selected structural indices. But with different colors of circles and clusters exhibiting different depths and trends. The Euler solutions, as seen on (Figs. 16 & 17), would give an idea about the depth estimate of the magnetic sources. The first map (N = 0) shows a very good clustering of circles in linear and curved fashions, indicating the nature of the probable contacts. The linear contacts may be the result of faults.

The Deduced subsurface structures from the Euler deconvolution of the RTP magnetic map Fig. (16) (contacts), N = 0, reflects that the deepest faults are at depth (820 m) and trend in the NNW-SSE and E-W directions especially at the southern and eastern parts of the study area. Meanwhile, the most shallower faults (0 – 350 m) are found in the northwestern and southeastern parts, as well as some parts in the mid of the mapped area. These faults take the N-S, NE-SW, E-W and NW-SE directions.

The contacts are structurally controlled, besides the depth estimates, as deduced from the colored circles, are in complete harmony with the regional component magnetic map. The second map (Fig.17) (N = 1) is a fingerprint to the first, but with more deep depths and linear clusters at different locations, suggesting the penetration of the interpreted faults to deep levels. The depth results obtained from the depth determination techniques reflect that the deepest faults (850 – 1150 m) are restricted in the southern, eastern and northern parts of the investigated area and they take the NNW-SSE, NE-SW and N-S directions. Meanwhile, the intermediate and shallow faults (0 – 850 m) are recorded in the northwestern and southeastern parts which trending in the NE-SW direction. Beside some small faults distributed in different localities allover the study area.

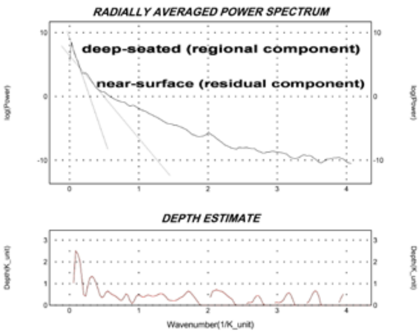

Fig. (9): Local radially averaged power spectrum curve for the interface determination of the RTP aeromagnetic contour map, G. ELmogarid Area, South Eastern Desert, Egypt.

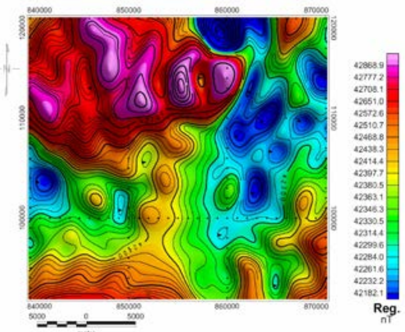

Fig. (10): Low-pass filtered (regional) magnetic component contour map, G. ELmogarid Area, South Eastern Desert, Egypt.

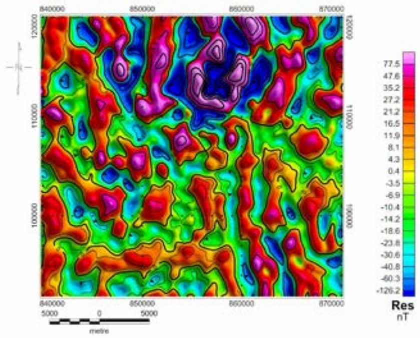

Fig. (11) High-pass filtered (residual) magnetic component contour map, G. ELmogarid Area, South Eastern Desert, Egypt.

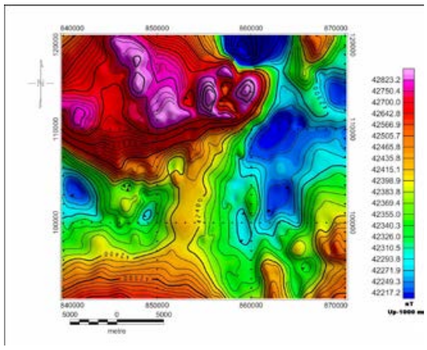

Fig. (12): Upward continuation of the RTP aeromagnetic contour map at (1.0 Km), G. ELmogarid Area, South Eastern Desert, Egypt.

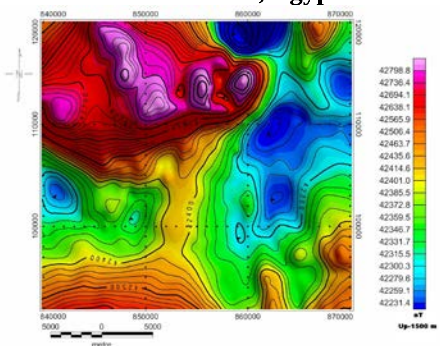

Fig. (13): Upward continuation of the RTP aeromagnetic contour map at (1.5 Km), G. ELmogarid Area, South Eastern Desert, Egypt.

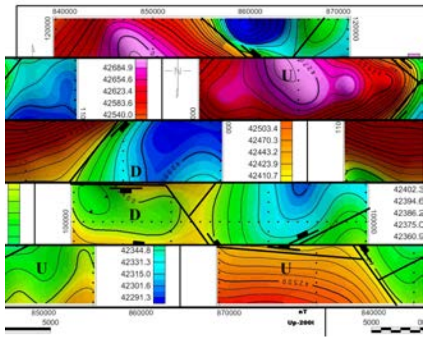

Fig. (14): Upward continuation of the RTP aeromagnetic contour map at (2.0 Km), G. ELmogarid Area, South Eastern Desert, Egypt.

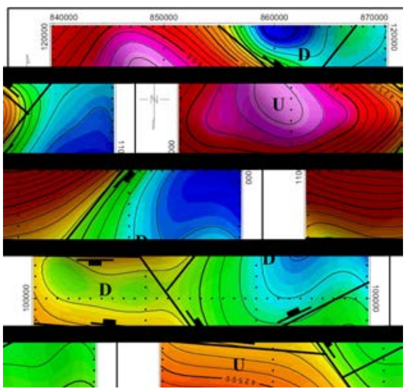

Fig. (15): Upward continuation of the RTP aeromagnetic contour map at (2.5 Km) ,G. ELmogarid Area , South Eastern Desert, Egypt.

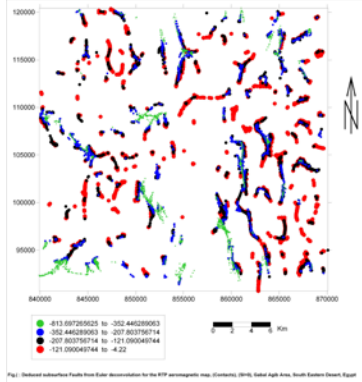

Fig. (16): Deduced subsurface faults from Euler deconvolution for the RTP aeromagnetic map, (Contacts), (N=0), G. ELmogarid Area, South Eastern Desert, Egypt.

The structural trends, that picked out from (Figs.16 & 17) can be arranged according to their importance in the E-W, N-S, NNW-SSE, NE-SW and NW-SE directions, which are close to the sequence inferred previously from the RTP magnetic map.

VI- Interpreted Magnetic Basement Structural Map:

Since the area under investigation is mainly represented by igneous and metamorphic rocks and having a great variety in their composition (acidic and basic rocks). These rocks were affected by various regional and local geologic structures of varying types, magnitudes, trends and locations. Due to the nature of the Precambrian basement rocks, which are occurred in the area under investigation it is expected that, faulting as a structural style is well-developed rather than any other structural element.

The rose diagram technique, as a simple and standard method for portraying the two dimensional patterns is to construct a frequency plot showing the percentage of trends lying in various direction ranges (Miller and Khan, 1962). The trends of the lineations were grouped in 10-degree classes, and their lengths and numbers within a class were summed up and calculated as a percentage of the total lengths or numbers of all trends. The frequency distribution was constructed with respect to direction (clockwise and anticlockwise from the north).

In the present study, the structural interpretation of the aeromagnetic survey data was carried out through the construction of two basement structural maps (Figs. 18 & 19) for the deep-seated and near-surface features, respectively, and the rose diagrams of the main lineament features (Fig. 20). These maps show the gross structural framework of the study area and display its main structural features.

Basically, the regional (deep-seated) magnetic basement structural map (Fig. 18) is constituted of large-scale compositional variations within the buried crystalline basement complex (intra-basement magnetic effects) and large-scale structural relief features (supra-basement magnetic effects). Meanwhile, the residual (near-surface) magnetic basement structural map comprises mainly the contributions of small scale (detailed) structural features of the magnetic basement complex. Both are constructed mainly depending on the close examination and integration of the various magnetic maps obtained through the application of different geophysical techniques. It is important to point out that, the tracing of structural elements on these maps was checked through the geological and geomorphological information available from the geological and topographical maps (Figs. 2&3) of the area under study in order to enhance the validity of interpretation.

The study area is dissected by numbers of normal faults, which are concomitant with wadis and drainage line, contacts or cutting through the country rocks. The faults mainly trend in the N-S, E-W, NNW-SSE, NW-SE and NE-SW directions.

The magnetic signatures of the interpreted regional and residual magnetic basement structural maps (Figs. 18 and 19) and the rose diagrams of the main lineament features (Fig.20) show several alternative high and low magnetic zones. The magnetic-low zones are supposed to represent structural lows (down-thrown blocks or grabens), while the magnetic-high zones, separating them are supposed to represent structural highs (up-faulted blocks or horsts). The distinct boundaries between these zones, with appreciably different magnetic characters, may indicate the presence of major basement faults and/or contacts. Besides, the sharp changes in the magnetic anomaly trends are indeed related to systematic structural lineaments representing faults. These magnetic structural lineaments, which heavily dissect the area under study, are shown on the two basement structural maps (Figs. 18 and 19).

The first look to the regional (deep-seated) magnetic basement structural map (Fig. 18) indicates that, the study area shows distinctive group of alternative up-thrown and down-thrown structural blocks, which extend from south to north with major E-W to NW-SE trends. These interfingering structures of high and low basement blocks are bounded from the western and eastern sides by a cluster of clysmic normal faults trending in the NNE-SSW and NE-SW directions. These bounding clysmic faults occasionally display a remarkable smooth rotation to the E-W and NW-SE directions.

The NNW-SSE to NW-SE trending high and low basement structures are highly dissected by a series of NE-SW trending diagonal faults. The NW-SE (clysmic) faults constitute with the NE-SW trending cross faults and the oblique ones (N-S and NNE-SSW) the overall structural pattern of the study area.

With respect to the residual (near-surface) magnetic basement structural map (Fig. 19) and the rose diagrams of the main lineament features (Fig.20), it can be concluded that, the structural elements dissecting the basement rocks at this map are highly intensive than those displayed at the deep-seated interface.

There is a distinct increase in the density and crowdness of these elements upwardly. However, this map (Fig. 19) and the rose diagrams of the main lineament features (Fig.20) show to a great extentsimilar structural features to those expressed by the regional magnetic basement structural map (Fig. 18), but with greater degree of complexity on the residual one. There are two major trends NNW-SSE and E-W trends. The interfingering between these two major trends forms horsts, grabens and step-like fault patterns, which build up the general structural configuration of the buried basement rocks. It seems that, the residual basement structural map produced a second-order NNW-SSE, E-W, NW-SE and NE-SW trends.

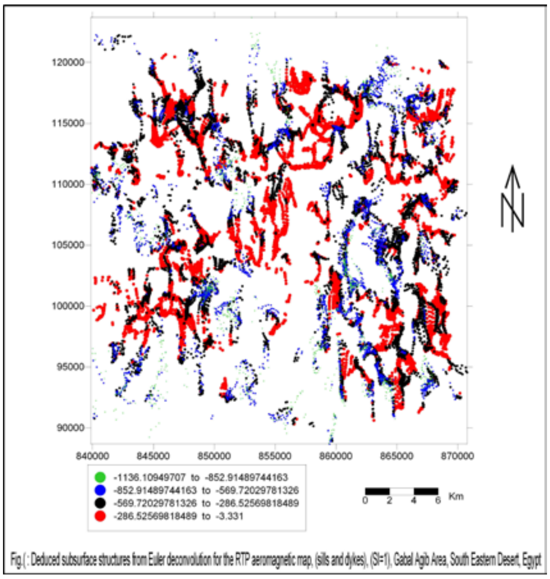

**Fig. (17): Deduced subsurface structures from Euler deconvolution for the RTP aeromagnetic map,
(sills and dykes), (N=1), G. ELmogarid Area, South Eastern Desert, Egypt.**

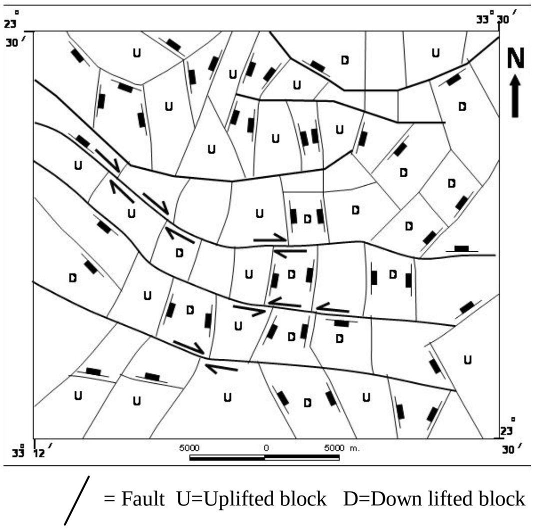

Fig. (18): Interpreted regional (deep-seated) magnetic basement structural map, G. ELmogarid Area, South Eastern Desert, Egypt.

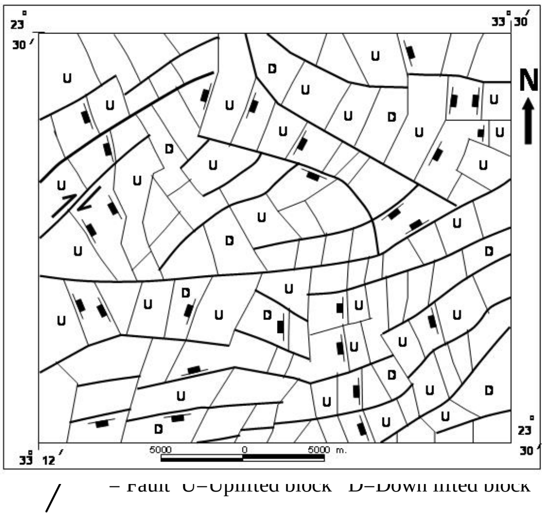

Fig. (19): Interpreted residual (near-surface) magnetic basement structural map, G. ELmogarid Area, South Eastern Desert, Egypt.

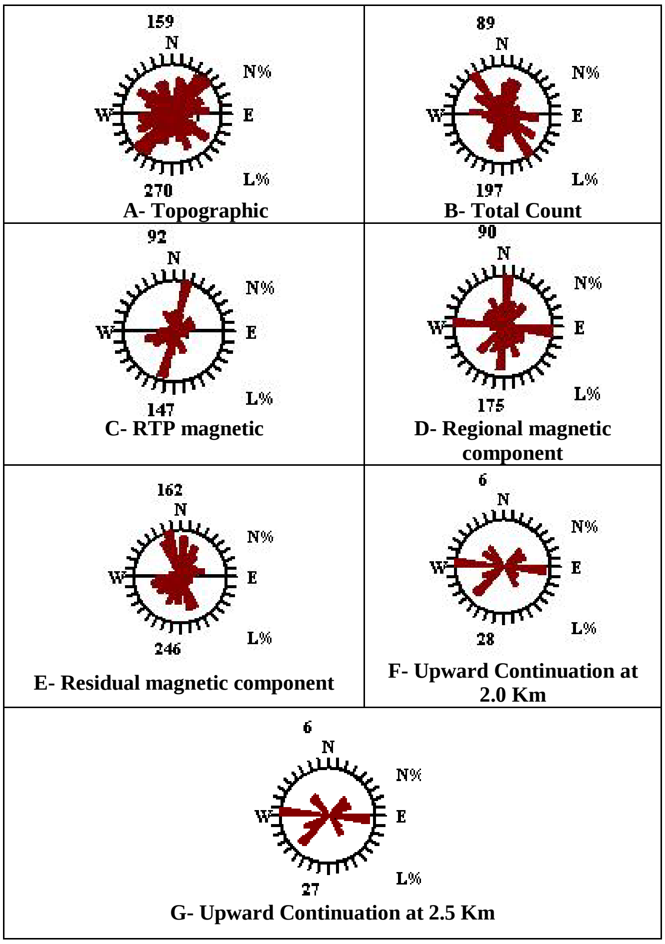

**Fig. (20): Rose diagrams, of the main lineament features, as deduced from the maps of:
A- Topographic, B- Total Count, C- RTP Magnetic, D- Regional Magnetic Component,
E- Residual Magnetic Component, F- Upward Continuation at 2.0 Km, G- Upward Continuation at 2.5 Km
Gabal El mogarid , South Eastern Desert , Egypt.**

The upward continued maps (Figs.14 & 15) for depths 2.0 and 2.5 km show that, the area become less in the density of the faults and appear that, the study area affected by two major faults trend in th the E-W directions two major faults trend in the the NW-SE direction and two major faults trends in NE-SW direction. These faults give uplifted and subsided blocks and they further give a graben shape nearly in the mid part of the western part of the mapped area.

CONCLUSION

Gabal El Mogarid area is located in the south Eastern Desert of Egypt, between latitudes 23° 30' & 23° 45' N and longitudes 33° 12' & 33° 30'. It covers a total surface area of about 840 Km^2. The delineation of the gross structural framework, was reached through the integration of some interpretation techniques applied to the aeromagnetic survey data. Two main average interfaces at depths 0.8 and 1.6 km below the measuring level were calculated by the computation of the local power spectrum of the aeromagnetic data. the band-pass filter technique produced the regional (deep-seated) magnetic source at 1.6 km and the residual (near-surface) magnetic source at 0.8 km.

The upward continuation computed at two levels (1.0 and 1.5 km) shows the existence of high and low magnetic zones and most of the residual bodies are removed. Meanwhile, the other upward continuations computed at the two levels (2.0 and 2.5 km) shows that, the large masses (anomalies) are bounded and separated from the others by NE and NW major faults.

The NNW, NW and NE trending faults are the three main trends affecting the distribution of the radioactive elements. The application of Euler Deconvolution technique determined the depths of the causative magnetic bodies. Two-basement tectonic maps at the two interfaces of depths (0.8 and 1.6 km) were constructed depending upon the integration of the results obtained from the magnetic data, aided by the compiled geologic information.

These two maps show a gradual increase in the density and crowdness of the interpreted magnetic structural lineaments upwardly from the deep-seated to the near-surface interfaces. The regional (deep-seated) faults are represented mainly by the N-S, E-W and NE trends faults, while the residual (near-surface) lineaments are characterized by a mosaic pattern and show different sets of fault system mainly trending in the NNW, N-S, NW and NE directions.

It could be concluded finally that, the application of radioactive and magnetic methods simultaneously to the lithology and structures, when related to the geologic information, represents a powerful tool in geological mapping, mineral exploration (both radioactive and associated non-radioactive), as well as environmental investigations.

REFERENCES

Aero Service, (1984): Final operational report of airborne magnetic/radiation survey in the Eastern Desert, Egypt. For the Egyptian General Petroleum Corporation, Cairo, Egypt. Aero Service, Houston. Texas, USA, six volumes.

Baranov, V. (1975): Potential fields and their transformations in applied geophysics. Geoexploration Monographs, Series L, No.6, Gebruder Brontrager, Berlin, Stuttgrart, Germany.

Baranov, V. and Naudy, H. (1964): Numerical calculation of the formula of reduction to the magnetic pole. Geophysics, Vol.29, pp.67-79.

Blakely, R.J. (1995): Potential theory in gravity and magnetic application. Cambridge University Press, Cambridge, UK.

Conoco Coral (1987): Geological map of Aswan, scale 1: 500,000. The Egyptian General Petroleum Corporation, 1 map.

Curits, C.E. and Jain, S. (1975): Determination of volcanic thickness and underlying structures from aeromagnetic map in the Silt area of Algeria. Geophysics, Vol. 40, No. 1, pp. 79-90.

El-Shazly, E.M. (1966) : Structural Development of Egypt, the Geol. Soc. of Egypt, 4th Annual Meeting, Cairo, Egypt, An extended abstract, pp.31-38.

Fouad, K.M., Ammar, A.A. and Meleik, M.L. (1987): Master curves for optimal reduction of total magnetic field data to the pole. Proceedings of the Fifth International Mathematical Seminar on Model Optimization in Exploration Geophysics, Free Univ. of Berlin, West Germany, pp.125-135.

Geosoft Package (1994): Geosoft mapping and processing system, Geosoft Inc. Toronto, Canada.

Hunting Geology and Geophysics, Ltd. (1967): Photogeological Survery Assessment of the mineral potential of the Aswan region : United Nation Development Program, United Arab Republic Regional Planning of Aswan, 138p.

Kearey, P. and Michael, B. (1994): Image processing of aeromagnetic data and integration with Landsat images for improved structural interpretation. Geophysics, Vol. 52, No. 7, pp. 875-884.

Mansour, S.E. (1985) : The relation of radioactivity to the geological features, Southeast Aswan, Egypt : Ph. D. Thesis, Al Azhar Univ., Cairo, Egypt.

Miller, R.I. and Khan, J.S. (1962): Statistical analysis in the geol. Sciences. Hohn Willey and Sons Inc., New York. USA, 429p.

Reid, A.B. (1995): Euler deconvolution, past, present and future. A Review. 65th Ann. Internat. Mtg., Soc. Expl. Geophys., Expanded Abstract, pp. 272-273.

Tasy, L.J. (1975): The use of Fourier series method in upward continuation with new improvements. Geophysical Prosp., Vol. 23, pp. 28-41.

Telford, W.M., Geldart, L. P., Sheriff, R. E. and Keys, D.A. (1990): Applied geophysics. Cambridge Univ. Press, 870p.